RSC Advances

# Fabrication of Nitrogen Doped Graphene Oxide Coatings: Experimental and Theoretical Approach for Surface Protection



| | |
|---|---|
| Journal: | *RSC Advances* |
| Manuscript ID: | RA-ART-10-2014-013470.R2 |
| Article Type: | Paper |
| Date Submitted by the Author: | 17-Jan-2015 |
| Complete List of Authors: | Madhankumar, A; King Fahd University of Petroleum and Minerals, Center of Research Excellence in Corrosion, Research Insitute<br>Rajendiran, Suresh; Sunchon National University, Sunchon, Chonnam, Department of Printed Electronics Engineering in World Class University (WCU) Program<br>Obot, I.B.; King Fahd University of Petroleum and Minerals, Dhahran, KSA-31261., Center of Research Excellence in Corrosion, Research Institute,<br>Gasem, Zuhair; King Fahd University of Petroleum and Minerals, Dhahran, KSA-31261., |
| | |

# Graphical Abstract

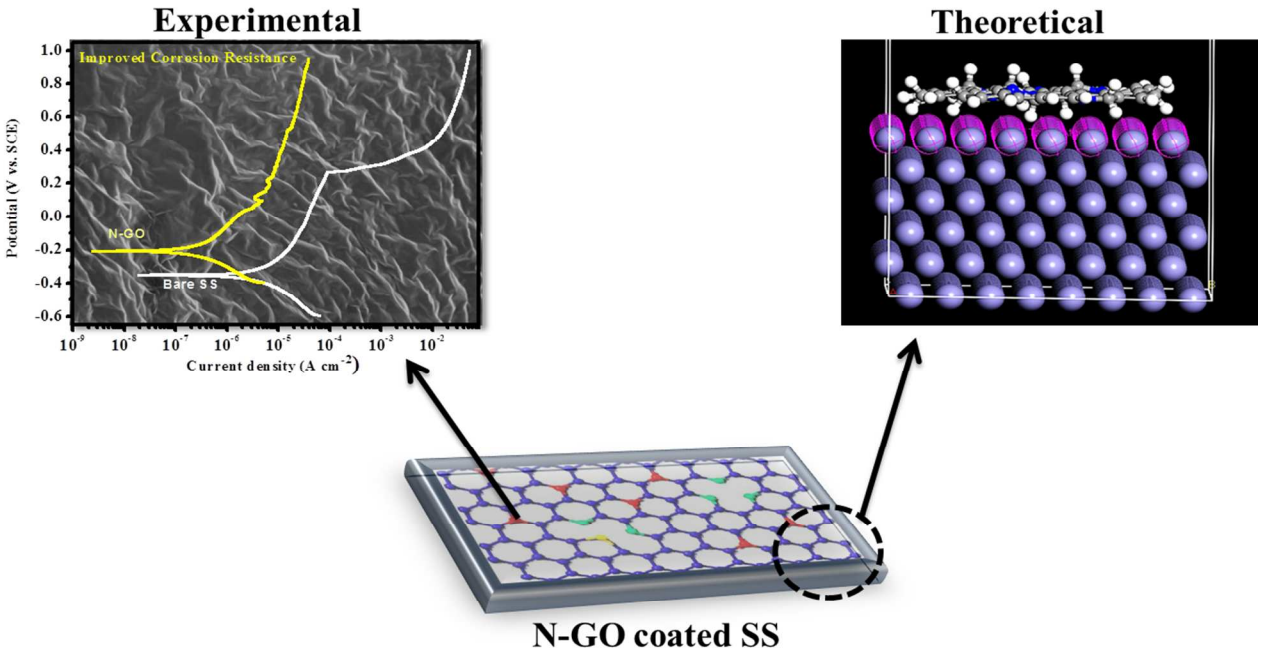

# Fabrication of Nitrogen doped Graphene Oxide Coatings: Experimental and Theoretical Approach for Surface Protection

**A. Madhan Kumar[a*], R. Suresh babu[b], I.B. Obot[a], Zuhair M. Gasem[a]**

[a]Center of Research Excellence in Corrosion, Research Institute,
King Fahd University of Petroleum and Minerals, Dhahran, KSA-31261.

[b]Department of Printed Electronics Engineering in World Class University (WCU) Program, Sunchon National University, Sunchon, Chonnam 540-742, Republic of Korea

**Abstract**

In this work, we present a simple strategy of fabricating an N-doped graphene oxide (N-GO) coating on stainless steel (SS) for protective application. Electrochemical, surface analytical and quantum chemical techniques were employed to characterize the synthesized coatings on SS surface. Graphene oxide (GO) and reduced graphene oxide (rGO) coating on SS were adopted for comparison. The downshift of G band in Raman spectra of N-GO corroborated the incorporation of N atoms and deconvoluted spectra of N1s revealed that N-GO coatings retain three types of nitrogen. The influence of N doping on the surface roughness and hydrophobicity of GO was investigated using surface topographic and contact angle measurements. An electrochemical corrosion study on the coatings indicated that N doping of GO enhances the corrosion resistance of SS in 3.5% NaCl solution more than GO and rGO. In order to describe the underlying mechanism, the adsorption energies of GO coatings with SS were computed using molecular dynamics simulation (MDS). The MDS result revealed that all the coating systems adsorbed in a parallel orientation on Fe surface. N-GO coating exhibited the strongest and the most stable chemisorbed interaction on SS when compared to GO and rGO.

**Keywords:** Graphene oxide; Coatings; Corrosion; Molecular dynamics simulation

*****Corresponding Author:

**Email:** madhankumar@kfupm.edu.sa **Phone:** +966538801789 **Fax:** +966538604818

## Introduction

Graphene, a single layer of $sp^2$-hybridized carbon atoms in a closely packed honeycomb structure is one of the emerging material of solution dispersible polyaromatic, two-dimensional carbon sheets. It has been the subject of intense widespread research for a decade due to its unique features such as high Young's modulus, fracture strength, thermal conductivity, mobility of charge carriers, and specific surface area. Regrettably, the poor solubility of graphene in both polar and non-polar solvents has greatly limited its preparation and further applications. However, Graphene oxide (GO) is hydrophilic in nature due to a great deal of oxygen functional groups on its basal plane and edges. Although GO has the same lamellar structure as graphene, it holds perhaps promising properties due to the functional groups, typically its good dispersion stability in aqueous and other organic solvents [1].

It was reported that the fairly poor conductivity of GO might hinder its efficient charge transfer [2]. Reduction of GO may partly recover the perfect graphene structure, being favorable to increasing its conductivity. However, the reduced GO often suffers from irreversible agglomeration and restacking due to van der Waals interactions, which adversely affects its electrochemical performances by reducing specific surface area [3]. Hence, doping/functionalization at the carbon basal planes and the edge sites have been introduced to overcome this limitation and opens up a new way for real-life applications. In general, substitutional doping of graphene with different atoms (e.g. B, N, S and Si) results in the disruption of the perfect $sp^2$ hybridization of the carbon atoms, hence locally encouraging substantial changes in their electronic properties.

Among the various potential dopants, nitrogen has attracted much attention because it is in comparable atomic size and contains five valence electrons available to form strong valence bonds with carbon atoms [4]. Thus, it can be easily introduced into the lattice of carbon to improve the electron-donor properties and enhance the binding ability of graphene. In particular, N-doping promises many fascinating properties and widespread potential in high-frequency semiconductor devices and enhanced catalysis for energy conversion and storage[5]. In addition, N-doping could also enhance the biocompatibility of carbon nanomaterials and therefore is favorable for biosensing applications [4].

Due to its chemically inertness and high durability, graphene as a corrosion protection coating is also one of the field which has generated a lot of interest among researchers and provides new insight in developing anticorrosive coating layers on a metal substrate [6]. Kirkland et al reported the electrochemical response of graphene-coated nickel and copper, whereby a graphene layer was shown to significantly reduce their corrosion rate [7]. Prasai et al have demonstrated that single-layer and multilayer graphene films can serve as corrosion-inhibiting coatings for Cu and developed quantitative models describing the passivation mechanism [8]. Soon-Yong Kwon et al have validated the excellent performance of acetone-derived graphene as corrosion inhibition coatings for Cu in a seawater environment [9].

Kang et al have recently achieved the enhanced oxidation resistance of Fe and Cu foils by coating them with reduced graphene oxide (rGO) sheets [10]. To the best of our knowledge, research on corrosion resistance of N-doped graphene oxide (N-

GO) and rGO coatings on stainless steel (SS) substrates has not been reported. In this present study, we have fabricated the N-GO and rGO coatings on SS substrate and investigated their potential use as corrosion inhibition in 3.5% NaCl solution using electrochemical methods such as potentiodynamic polarization and electrochemical impedance spectroscopy (EIS) measurements

## 2. Experimental Procedure

### 2.1. Materials and methods

420 SS was used as a substrate and the composition was (in wt. %) 12 Cr - 0.75 Ni - 1 Si - 0.01 P - 0.15 C - 1 Mn - balance Fe. Prior to each electrochemical experiment, the working electrode was mechanically ground with abrasive paper using grit sizes starting from 600 to 2400 in sequence and cleaned in 1:1 acetone/ethanol mixture in an ultrasonic bath to remove impurities, rinsed with water and then dried in air in order to degrease and clean the surfaces to improve the adhesion of the coating.

The GO was prepared by a modified Hummer's method [11]. Briefly, 5 g of graphite and 3.5 g of $NaNO_3$ were placed in a round bottom flask. $H_2SO_4$ (350 mL) was added with stirring in an ice-bath environment. Ten grams of $KMnO_4$ was added slowly with vigorous stirring for 2 h in room temperature and the flask was kept at room temperature for 6 days. 200 mL of 5 wt. % $H_2SO_4$ was then added to the mixture and kept at 98 °C under fluxing for 2 h. When temperature was reduced to 50 °C, 10 mL of $H_2O_2$ (30 wt. % aqueous solution) was added to terminate the reaction. The resultant mixture was purified by centrifugation and washing with 10% HCl, water and then methanol. The dark precipitation was collected and freeze dried for 2 days.

N-GO (300 mg) was prepared by heat treatment of the GO loaded in a ceramic boat in a SiC tube furnace at 400 °C for 2 h in a gas mixture of comprising $NH_3$(10%) and Ar (90%) with a total flow rate of 500 mL $min^{-1}$. For comparison rGO was prepared under the same condition at 400 °C for 2 h in an Ar atmosphere.

The 0.2 mg/ml of synthesized N-GO was dispersed in anhydrous ethanol by sonication (40 kHz) for 3 h. A dispersion of 250 µL was spin-coated onto SS substrates with the dimensions of 10×10 $cm^{2.}$ The rotation speed was vital and was optimized at 100 rpm for a uniform and well-spread coating. An increase in rotation speed caused irregular spreading and coating. The N-GO coated SS substrates were dried at 80 °C overnight, followed by drying under vacuum at 100 °C for 5 h. Pure GO and rGO coatings were also prepared in the same condition as mentioned above.

### 2.2. Characterizations

The surface morphology of GO, rGO and N-GO was examined using scanning electron microscopy (SEM). The associated energy-dispersive X-ray spectrum (EDX) provided qualitative information about surface elemental composition. The surface topography was analyzed with atomic force microscopy (AFM) using the NANO Station II Surface Imaging Systems. The images were acquired by non-contact mode using Au coated silicon cantilevers with a spring constant of 1.6 N/m at a resonance frequency of 26 kHz measured at room temperature. The chemical composition of the coatings was studied by Fourier

transform infrared spectroscopy (FT-IR, JASCO, FT/IR-6100). The phase identification of the GO coatings was performed using X-ray diffraction analysis (XRD) (RINT2500, Japan; CuKα, 40 kV, 20 mA) over a scattering angle range of $20° \leq 2\theta \leq 80°$ at a 2θ step of 0.02°. X-ray photoelectron spectroscopy (XPS) (Thermo Scientific, ESCALAB-250Xi) was employed to determine the chemical composition of N-GO coatings. The XPS spectra were recorded using Al Kα radiation (1486.6 eV) as excitation source. The take-off angle θ of the emitted photoelectrons was adjusted to 45° with respect to the surface normal.

Contact angles of the substrates were determined by contact angle goniometry at 25 °C using an Attension optical goniometer interfaced with image-capture software by injecting a 2 µL liquid drop. Deionized water was used as the test liquid. To obtain reliable contact angle data, five droplets were dispensed at different regions of the bare and coated SS substrates.

**2.3 Electrochemical measurements**

Electrochemical investigations of bare and coated SS substrates were performed in 3.5% NaCl solution using potentiodynamic polarization and electrochemical impedance spectroscopy (EIS). The anodic and cathodic polarization curves were measured by varying the electrode potential between –250 mV and +1000 mV at open circuit potential (OCP) with a constant sweep rate of 1 mV $s^{-1}$. The corrosion rates were evaluated by Tafel extrapolation and the results are presented in mils per year (mpy). EIS data were recorded over the frequency range of 10 kHz–1 mHz, with acquisition of 10 points per decade, with a signal amplitude of 10 mV at OCP. The analysis of the impedance spectra was evaluated by fitting the experimental results to equivalent circuits using the non-linear least-square fitting procedure. All measurements were repeated at least three times until good reproducibility of the results was obtained.

## 3. Results and Discussions

**3.1. FTIR analysis**

FTIR spectra of GO, rGO and N-GO shown in Figure S1 as supplementary information revealed that the chemical modification of the GO structure occurred after $NH_3$/Ar treatment. The unmodified GO showed O-H, C=O, aromatic C=C, peaks at 3430 $cm^{-1}$, 1720 $cm^{-1}$ and 1631 $cm^{-1}$ respectively (curve a) [12]. The O-H stretching and deformation peaks around 3400 $cm^{-1}$, and 1400 $cm^{-1}$, respectively greatly reduced after the thermal treatment of Ar. In addition, there was a significant decrease in C=O stretching peak (curve b). Similarly, substantial changes were found in the fingerprint region (2000–800 $cm^{-1}$) of the spectrum indicating the involvement of nitrogen in the bonding structure of N-GO (curve c). The C=N stretching vibration band at 1540 $cm^{-1}$ is assigned to the pyridine or pyrrolic type ring in the graphene. Furthermore, a broad peak at ~1100 $cm^{-1}$ appeared, probably due to the formation of N-C bonds [13, 14].

**3.2 XRD analysis**

The XRD patterns for GO, rGO, and N-GO are shown in Figure S2 as supplementary information. The GO showed a significant (002) peak at 11.43°, and a d-spacing of 0.77 nm. The large interlayer distance of the GO was attributed to the presence of hydroxyl, epoxy, and carboxyl groups. Following the reduction, the sharp (002) peak of GO disappeared; the (002) peak of rGO was observed at 22.42°, with an interlayer distance of 0.39 nm, indicating that the rGO removed some of the oxygen-containing functional groups. The XRD pattern for the N-GO showed that the GO structure was successfully reduced and doped with nitrogen, with the same d-spacing of 0.39 nm. In addition, the N-GO peaks changed little at $2\theta = 22.21°$, could be assigned to the (002) graphite structure, similar to the XRD results for the rGO.

**3.3 Raman spectroscopic studies**

The N doping of GO can be further supported by Raman analysis. As shown in Figure 1a, each sample shows D and G bands at ~1343 and 1580 $cm^{-1}$, respectively. The relative intensity ratio of these bands ($I_D/I_G$) was also estimated and it was about 0.93, 1.08 and 1.08 for GO, rGO and N-GO samples, respectively. The intensity of the D band is strongly associated with the degree of disorderliness of graphene, while the G band corresponds to the first-order scattering of the stretching vibration mode $E_2g$ observed for $sp^2$ carbon domains. The rGO and N-GO showed apparently higher $I_D/I_G$ ratio than the GO. This suggests that the rGO and N-GO sheets are more disordered than the pristine GO, which is consistent with a previous report[15].

Moreover, remarkable changes were observed in the peak positions, which were shifted to lower frequencies. With the doping of N, the position of G bands of N-GO shifted from 1588.5 $cm^{-1}$ to 1582 $cm^{-1}$. The D band and G band of NGO sheets shifted because of the structural distortion of GO caused by the different bond distances of C-C and C-N. The downshift of G band peak position in N-GO could be attributed to the fact that the incorporation of N atoms leads to n-doping effect. This observation is similar to previous reports that the interaction between graphene and electron-donating species causes downshifted G band peak [16].

**3.4 XPS studies**

XPS analysis is an excellent and commonly used technique to examine the features of nitrogen atoms in graphene materials. The survey spectrum of N-GO is shown in Figure S3. Distinctive C1s, N1s and O1s peaks can be seen from the survey scan. The amount of nitrogen incorporated in the N-GO was found to be 10.8 at%. The peak centered on 400 eV, which corresponds to the N1s region; Figure 1b shows the deconvoluted N1s region of N-GO. When a nitrogen atom is doped into graphene, it generally has three common bonding configurations within the carbon lattice, including quaternary N (or graphitic N), pyridinic N, and pyrrolic N. Specifically, pyridinic N bonds with two C atoms at the edges or defects of graphene and donates one p electron to the π system. Pyrrolic N denotes to N atoms that donate two p electrons to the π system, though unnecessarily

bond into the five-membered ring, as in pyrrole. Quaternary N denotes to N atoms that substitute for C atoms in the hexagonal ring.According to the bond configuration and the location in the graphene crystallites, it has been reported that the pyridine like nitrogen atoms are more suitable to coordinate with the transitional metals and form the active sites [17,18]. However, it is impractical to produce pyridinic nitrogen only, because of the autonomous transformation between the pyridinic and quaternary nitrogen during the thermal treatment. Our results indicated the existence of three types of nitrogen and the high-resolution N1s could be deconvoluted into three components such as pyridinic N (N in 6-membered ring), pyrrolic N (N in 5-membered ring) and quaternary/graphitic N (N in graphene basal plane) [19].

**3.5 Surface characterization**

Figure 2 displays the GO, rGO and N-GO coatings on SS substrates. SEM images of GO coated SS exhibited a continuous and a compact GO layer with a few defects and cracks, which suggests that the distribution of graphene sheets on SS surface was not homogeneous in nature. On the other hand, rGO coated SS were well-exfoliated with majority of the flakes being only a few layers thick and several micrometers in diameter. N-GO coating exhibits wrinkles or wavy features, which can be ascribed to the hexagonal AB stacking order, that usually originates during the process of oxidation of graphite layers [20]. In addition, the high magnification SEM image of N-GO coating illustrates the typical bright wrinkles on the surface. The N doping can also be confirmed by the EDX spectra as shown in Figure S4. An obvious N peak can be clearly detected in each area of the N-GO. The elemental concentration of N in N-GO is found to be 11.62%, which is almost close to the determined value (10.80%) by XPS.

Three dimensional AFM topographic images of the GO, rGO and N-GO coatings are shown in Figure 3. It can be seen from the topographic images that all GO coatings exhibited exfoliated GO sheets with randomly distributed in nature. AFM images confirm that rGO and N-GO comprises of multi-layered arrangements of flakes. Further, rGO and N-GO samples have lateral dimensions of several micrometers and a thickness of 1–3 nm, which is characteristic of a fully exfoliated graphene oxide sheet. Moreover, it is observed from the AFM images that the N-GO sheet has higher flakes with rougher edges than rGO and GO coatings. AFM analyses disclose the same morphology of rGO and N-GO as that obtained from the SEM measurements**.**

**3.6 Contact angles measurements**

Figure 4 displays the contact angle results of GO, rGO and N-GO GO coatings on SS substrates. It can be seen that N-GO coated SS substrate was hydrophobic while the GO and rGO coated SS were hydrophilic. The observed increase in the air/water contact angle from 42.5° for GO to 121.5° for N-GO is accompanied with the surface chemistry modification due to the doping of nitrogen on GO. Conversely, the increase in the surface roughness has also contributed to the observed hydrophobicity.

This result confirmed that the nitrogen doped GO coating offers best hydrophobic water repellent coating to prevent oxidation and corrosion of SS substrates under service in stringent environment.

**3.7 Electrochemical corrosion analysis**

Figure 5 displays the potentiodynamic polarization curves of bare and coated SS which show obvious and marked differences. As a preliminary remark, the typical potentiodynamic curve of the bare SS displays an active dissolution followed by a region with tendency to passivation between 500 and 1000 mV (SCE). The value of corrosion potential ($E_{corr}$) is found to be about – 346 mV (SCE) with a corrosion current density ($j_{corr}$) of 5.660 $\times 10^{-6}$ A $cm^{-2}$, demonstrating that it is more prone to corrosion. Comparing polarization curves, the polarization curves of coated SS substrates are quite different from that of the bare SS. In the case of GO coatings on SS, $E_{corr}$ was slightly shifted and there was shift in $j_{corr}$, which suggests that GO coating provide protection for the SS substrates. On the other hand, rGO and N-GO coated SS substrates displayed obvious tendency to shift the $E_{corr}$ in more positive values combined with an increase in the passive range. Further, rGO and N-GO coated SS exhibited relatively constant current density value ($10^{-9}$ – $10^{-5}$ A $cm^{-2}$) in the whole examined potential domain. This result reveals the higher chemical inertness and stability of the coating in the aggressive medium. In particular, N-GO coating caused an extremely large positive displacement in $E_{corr}$ and substantial reduction of $j_{corr}$ when compared to GO and rGO. This result confirms the tendency of the N-GO coating to inhibit penetration of aggressive chloride ions into the underlying metal.

The kinetic parameters of the Tafel curves are given in Table 1. As shown in Table 1, the protection efficiency (η) for N-GO is calculated to be 98.85%, which is much higher than the protection efficiency of GO. The corrosion rate (v) is recognized to significantly reduce after the addition of the nitrogen in GO coatings. These findings point to the fact that the N-GO coated on SS efficiently protects the substrate and enhance the corrosion resistance due to the homogeneous distribution and relatively less porous surface of N-GO coatings with hydrophobic character preventing the permeation of electrolyte to the SS substrate.

EIS spectra for bare and coated SS substrates in 3.5% NaCl solution are presented as Bode plots in Figure 6. From the Bode spectrum, it is that bare SS displays only one relaxation time. However, after coating SS substrate with GO coatings, the spectrum shows a different Bode plot, which reveals that the substrate response can be composed of two relaxation times: the one at higher frequencies can be accompanied with the coating's response resulting from the penetration of the electrolyte through pores or cracks; the second one at low frequencies is a consequence of corrosion processes affecting the substrate [21].

Equivalent circuit configuration is represented in Figure S5, which can be used to describe the electrochemical behavior of bare and coated SS substrates. Different parameters related to impedance measurement were derived by curve fitting method and these are summarized in Table 2. An equivalent circuit consisting of a resistor connected in series

to a parallel connected resistor and capacitor for bare SS is shown in Figure S5a. On the other hand, a circuit of a resistor connected in series to a parallel connected resistors and capacitors for coated SS is displayed in Figure S5b. In these equivalent circuits, $R_s$, $R_{ct}$, $R_f$, $Q_{dl}$, and $Q_f$ represent solution resistance, charge transfer resistance, film resistance, constant phase element of double layer and constant phase element of the film, respectively. In addition, RE, CE, WE represent reference, counter and working electrode, respectively. A constant phase element (CPE) was used instead of capacitance due to the non-pure capacitance in the real electrochemical process. The CPE impedance is described by the following equation:

$$Z_{CPE} = 1/Y_o(J\omega)^n \quad (2)$$

where, $\omega$ is the frequency and $Y_o$ is the capacitance of the system. For a constant phase element, the exponent n is less than one [22]. Typically, n is close to 1, representing a capacitive characteristic of the interfaces. As seen in Table 2, the $R_{ct}$ value of the coated SS increased from 5.93 $k\Omega\ cm^2$ for bare to 21.38, 96.66 and 218.34 $k\Omega\ cm^2$ for the GO, rGO and N-GO coated SS substrates, demonstrating the improved and significant corrosion resistance of the coating . Further, the n values of rGO and N-GO coatings closed to 1 (ideal capacitor) indicate that both compact and defect free layers are highly insulating and resistant. On the other hand, the lower n value of GO coated SS proves that it has some defects and cracks, thus allowing $Cl^-$ ion from solution and is prone to corrosion on SS. Based on the above results, it can be concluded that nitrogen doped graphene oxide coatings exhibited superior corrosion protection performance than GO and rGO coatings on SS substrates.

**3.8 Theoretical study**

In order to gain detailed insights into the reactivity and stability of GO coatings on SS at the molecular level, theoretical studies using molecular dynamics simulation were employed. The interaction between the graphene coatings represented by graphene oxide (GO), reduced graphene oxide (rGO) and nitrogen doped graphene oxide (N-GO) and stainless steel represented by Fe (110) surface was investigated by performing Monte Carlo simulations using the adsorption locator module in the Material Studio 6.0 software [23]. The calculation was carried out using the condensed-phase optimized molecular potentials for atomistic simulation studies (COMPASS) force field. Before simulations, the Fe (110) plane was first cleaved from Fe crystal, the surface was then optimized to the energy minimum. The Fe (110) plane was next enlarged to a (10 × 8) supercell. After that, a vacuum slab with 4.0 nm thickness was built above the Fe (110) plane. At the same time, representative molecular structures of GO, rGO and N-GO molecules were also built and optimized (Figure 7). The atom-based method with a cutoff of 1.55 nm was applied to compute the non-bonds van der Waals and Coulomb interactions. Simulation annealing using Metropolis Monte Carlo method was used to sample possible configurations by carrying out Monte Carlo searches of the configuration space of the additives on the iron surface system as the temperature is gradually decreased. In this study, the automated temperature control was adopted and 100 temperature cycles were employed for each run.

The total energy, average total energy, van der Waals energy, electrostatic energy and intramolecular energy for (a) GO, (b) rGO and (c) N-GO adsorbed on Fe (110) surface were calculated by optimizing the whole system and are presented in Figure 8. The adsorption energy distribution of (a) GO/iron system (b) rGO/Iron system and (c) N-GO/Iron system are depicted in Figure 9. The most stable adsorption configurations of the systems under investigation are shown in Figure 10. The corresponding values for the outputs and descriptors are listed in Table 3. The parameters include total energy of the substrate–adsorbate configuration, which is defined as the sum of the energies of the adsorbate components, the rigid adsorption energy, and the deformation energy. It is well known that the potential energy does not have any unit during theoretical investigation[24]. The substrate energy (i.e., Fe (110) surface) is taken as zero. Moreover, adsorption energy reports the energy released (or required) when the relaxed adsorbate component was adsorbed on the substrate. The adsorption energy is defined as the sum of the rigid adsorption energy and the deformation energy for the adsorbate component. The rigid adsorption energy reports the energy released (or required) when the unrelaxed adsorbate component (before the geometry optimization step) was adsorbed on the substrate. The deformation energy reports the energy released when the adsorbed adsorbate component was relaxed on the substrate surface [25, 26]. Table 3 also gives (d*E*ad/dNi), which reports the energy of substrate–adsorbate configurations where one of the adsorbate components has been removed.

It is quite clear from Table 3, that the adsorption energies of the coatings on iron surface increased in the order GO < rGO < N-GO. Although rGO had a little bit higher negative adsorption energy than N-GO, it total energy was more positive (Table 3). This makes it less stable on the iron surface than N-GO. Highest negative adsorption energy indicates the system with the most stable and stronger adsorption [27-29]. Also by close examination of Figure 10, it could be seen that all the coating molecules adsorbed nearly parallel to the iron surface with N-GO been adsorbed at the best parallel position. This parallel adsorption is due to the donation of the π-electrons of the six membered rings and the lone pair of electrons of the hetero-atoms making up the coating structures to the iron unfilled d-orbital. These form strong chemisorbed bond and therefore strong coating on the stainless steel surface protecting the stainless steel from corrosion. This theoretical study is in agreement with experiment results.

**4. Conclusions**

Nitrogen doped graphene oxide coatings were successfully prepared on SS substrates. XRD pattern for the N-GO indicated that the GO structure was successfully reduced and doped with nitrogen, with the same d-spacing of 0.39 nm. Raman spectral studies revealed that the doping of N in GO causes shift in D band and G band due to the structural distortion of GO caused by the different bond distances of C–C and C–N. Deconvoluted XPS spectra of N1s confirms the presence of three types of nitrogen namely, pyridinic N (N in 6-membered ring), pyrrolic N (N in 5-membered ring) and graphitic N (N in graphene basal plane). Further, surface characterization demonstrates that N-GO coatings exhibited the typical bright wrinkles on the

surface which was rougher than other coatings. The N doped graphene coating exhibits robust corrosion resistance and protect steel surface in stringent chloride environment. Thus, it was concluded that the application of N-GO coatings is viable and can find promising application in the prevention of corrosion in industries.

**Acknowledgments**

The authors gratefully acknowledge King Fahd University of Petroleum and Minerals (KFUPM) for providing the facilities for the research.

**Reference**

1. D. Chen, H.B. Feng, J.H. Li, *Chemical Review*, 2012,112, 6027-6053.

2. Y. Yao, X.D. Chen, J.F. Zhu, B.Q. Zeng, Z.Q .Wu, X.Y. Li, *Nano Research Letters*, 2012,7,1-7.

3. C. K. Chua, M. Pumera, *Chemical Society Review*, 2014,43,291-312.

4. Y. Wang, Y.Y. Shao, D.W. Matson, J.H. Li, Y.H. Lin, *ACS Nano*, 2010,4, 1790-1798.

5. T. Kuila, A.K. Mishra, P. Khanra, N.H. Kim, J.H. Lee, *Nanoscale*, 2013,5,52-71.

6. M. Schriver, W. Regan, W.J. Gannett, A.M. Zaniewski, M.F. Crommie, A.Zettl, *ACS Nano*, 2013,7,5763-5768.

7. N.T. Kirkland, T. Schiller, N. Medhekar, N. Birbilis, *Corrosion Science*, 2012,56,1-4.

8. D. Prasai, J.C. Tuberquia, R.R. Harl, G.K. Jennings, K.I. Bolotin, *ACS Nano*, 2012,6,1102-1108.

9. J.H. Huh, S.H. Kim, J.H. Chu, S.Y. Kim, J.H. Kim, S.Y. Kwon, *Nanoscale*, 2014,6, 4379-4386.

10. Kang D, J.Y. Kwon, H. Cho, J.H. Sim, H.S. Hwang, C.S. Kim, et al. *ACS Nano*, 2012,6, 7763-7769.

11. H. Kim, D.H. Seo, S.W. Kim, J. Kim, K. Kang, *Carbon*, 2011,49,326-332.

12. S. Park, D.A. Dikin, S.T. Nguyen, R.S. Ruoff, *Journal of Phyical Chemistry C*, 2009,113,15801-15804.

13. Z. Lin, G. Waller, Y. Liu, M. Liu, C-P. Wang, *Advance Energy Mateials*, 2012 2,884-888.

14. Y. Jia-lin, C.Gui-jiao, C. Jun, Y. Wei, X. Bang-huy, Y. Ming-bo, *New Carbon Materials*, 2012, 27,370-376.

15. M. Li, Z.S. Wu, W.C. Ren, H.M. Cheng, N.J. Tang, W.B. Wu, et al. *Carbon*, 2012,50,5286-5291.

16. H.W. Mi, Y.L. Li, P.Y. Zhu, X.Y. Chai, L.N. Sun, H.T. Zhuo, et al. *Journal of Materials Chemistry A*, 2014,2,11254-11260.

17. Z.H. Sheng, L. Shao, J.J. Chen, W.J. Bao, F.B. Wang and X.H. Xia, *ACS. Nano*, 2011, 5, 4350-4358.

18. Tao Yang, Guiquan Han, *International Journal of Electrochemical Science*, 2012, 7, 10884 - 10893.

19. Y. Wang, Y.Shao, D. W. Matson, J. Li, Y. Lin, *ACS Nano*, 2010, 4, 1790- 1798.

20. H.K. Jeong, Y.P. Lee, R. Lahaye, M.H. Park, K.H. An, I.J. Kim, et al. *Journal of American Chemical Society*, 2008,130,1362-1366.

21. A. Madhankumar, Suresh Ramakrishna, P. Sudhagar, Hyongbum Kim, Yong Soo Kang, I. B. Obot and Zuhair Mattoug Asad Gasem, *Journal of Materials Science*, 2014, 49,4067–4080.

22. A. Madhankumar, S. Nagarajan, N. Rajendran, T.Nishimura, *Journal of Solid State Electrochemistry*, 2012, 16, 2085-2093.

23. A, Madhankumar, E. Thangavel, S. Ramakrishna, I.B. Obot, H.C. Jung, K.S. Shin, et al. *RSC Advances*, 2014,4,24272-24285.

24. L. Guo, S. Zhu, S. Zhang, Q. He, W. Li, *Corrosion Science* 2014, 87, 366-375.

25.K.F. Khaled, *Journal of Chimica Acta, 2012*, 1, 59-65.

26. K.F. Khaled, *Journal of Applied Electrochemistry*, 2011, 41, 423-433.

27. I.B. Obot, S.A. Umoren, Z.M. Gasem, R. Suleiman, B. El Ali, *Journal of Industrial and Enginnering Chemistry*, 2014, DOI: 10.1016/j.jiec.2014.05.049.

28. I.B. Obot, Z.M. Gasem, *Corrosion Science*, 2014, 83,359-366.

29. M.M. Kabanda, I.B. Obot, E. Ebenso, *International Journal of Electrochemical Science*, 2013,8,10839–10850.

**Figure Captions**

**Figure 1** a) Raman Spectra of GO coatings and b) XPS deconvolution spectra of N1s for N-GO coatings

**Figure 2** SEM images of (a) GO, (b) rGO (c) N-GO in low magnification and (d) N-GO in high magnification coatings on SS substrates

**Figure 3** AFM topographic images of (a) GO, (b) rGO and (c) N-GO coatings on SS substrates

**Figure 4** Contact angle results of GO, rGO and N-GO coatings on SS substrates

**Figure 5** Potentiodynamic polarization curves of (a) bare SS (b) GO, (c) rGO and (d) N-GO coatings

**Figure 6** (a) Bode impedance plot and (b) Bode phase angle plot of (1) bare SS (2)GO, (3)rGO and (4) N-GO coatings

**Figure 7** Optimized molecular structures of (a) GO, (b)rGO and (c) N-GO.

**Figure 8** Total energy distribution for (a) GO/iron system (b) rGO/Iron system and (c) N-GO/Iron system ( (i) Intramolecular energy (ii) Electrostatic energy (iii) Total energy (iv) Average total energy and (v) van der Waals energy ).

**Figure 9** The adsorption energy distribution of (a) sorbate GO of GO/iron system (b) sorbate rGO of rGO/Iron system and (c) sorbate N-GO of N-GO/Iron system.

**Figure 10** The most stable adsorption configuration of (a) GO (b) rGO, (c) N-GO on Fe (110).

**Table Captions**

**Table 1** Tafel parameters for bare and coated SS substrates ($E_{corr}$ - corrosion potential, $j_{corr}$ - Corrosion current density, $\beta_a$ - anodic slope, $\beta_c$ - cathodic slope, $\eta$-protection efficiency and $v$-corrosion rate)

**Table 2** EIS parameters for bare and coated SS substrates ($R_s$ - solution resistance, $R_{ct}$ - charge transfer resistance, $Q_{dl}$ - constant phase element of double layer capacitance, $Q_f$ - constant phase element of filim capacitance, $n_{dl}$ - heterogeneous factor for $Q_{dl}$, $n_f$ - heterogeneous factor for $Q_f$)

**Table 3** Outputs and descriptors calculated by the Monte Carlo simulation for adsorption of GO, rGO and N-GO on Fe (110) (in kJ/mol)

**Figure 1**

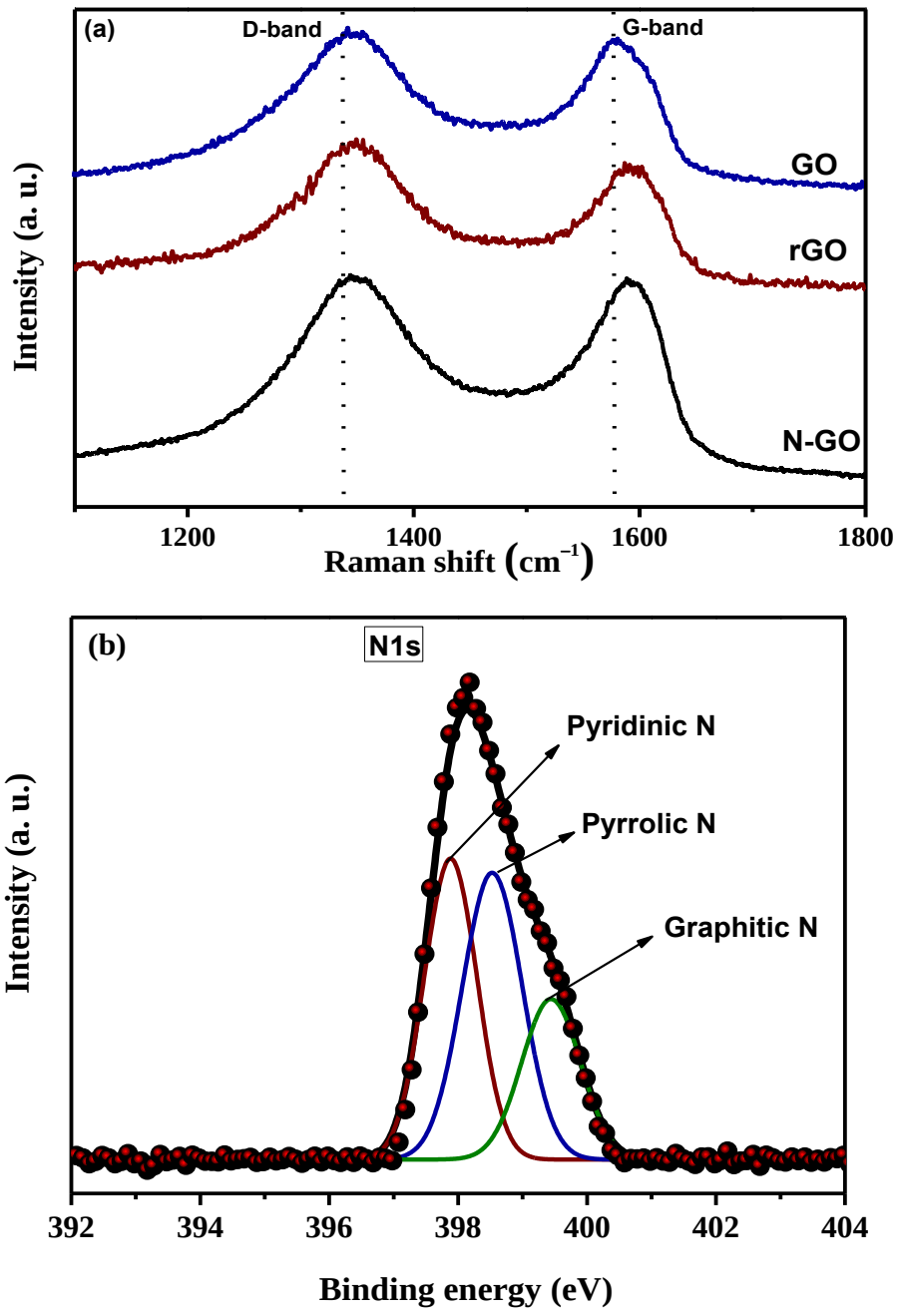
(a)
D-band
G-band
GO
rGO
N-GO
Intensity (a. u.)
1200
1400
1600
1800
Raman shift (cm$^{-1}$)
(b)
N1s
Pyridinic N
Pyrrolic N
Graphitic N
Intensity (a. u.)
392
394
396
398
400
402
404
Binding energy (eV)

**Figure 2**

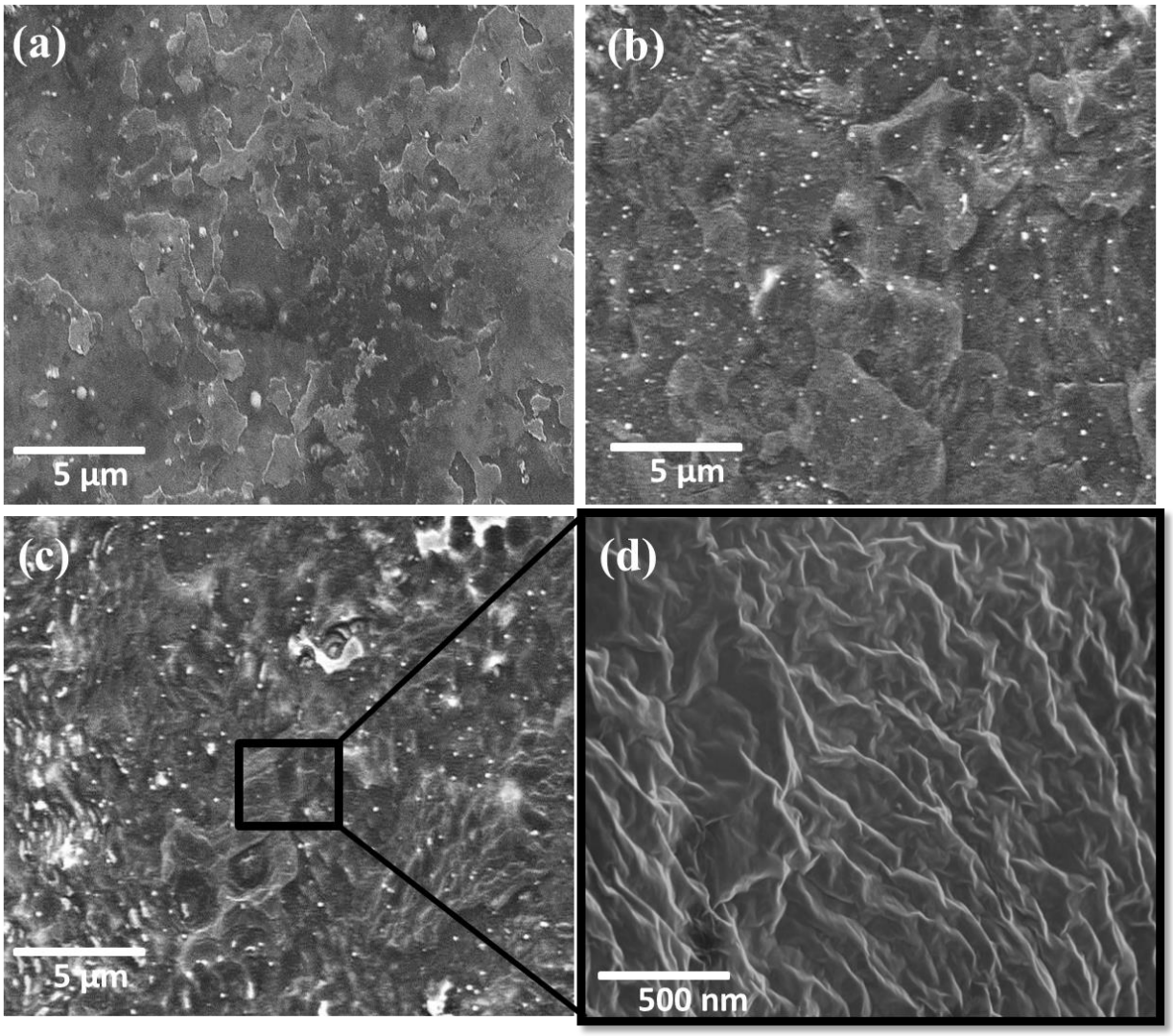

**Figure 3**

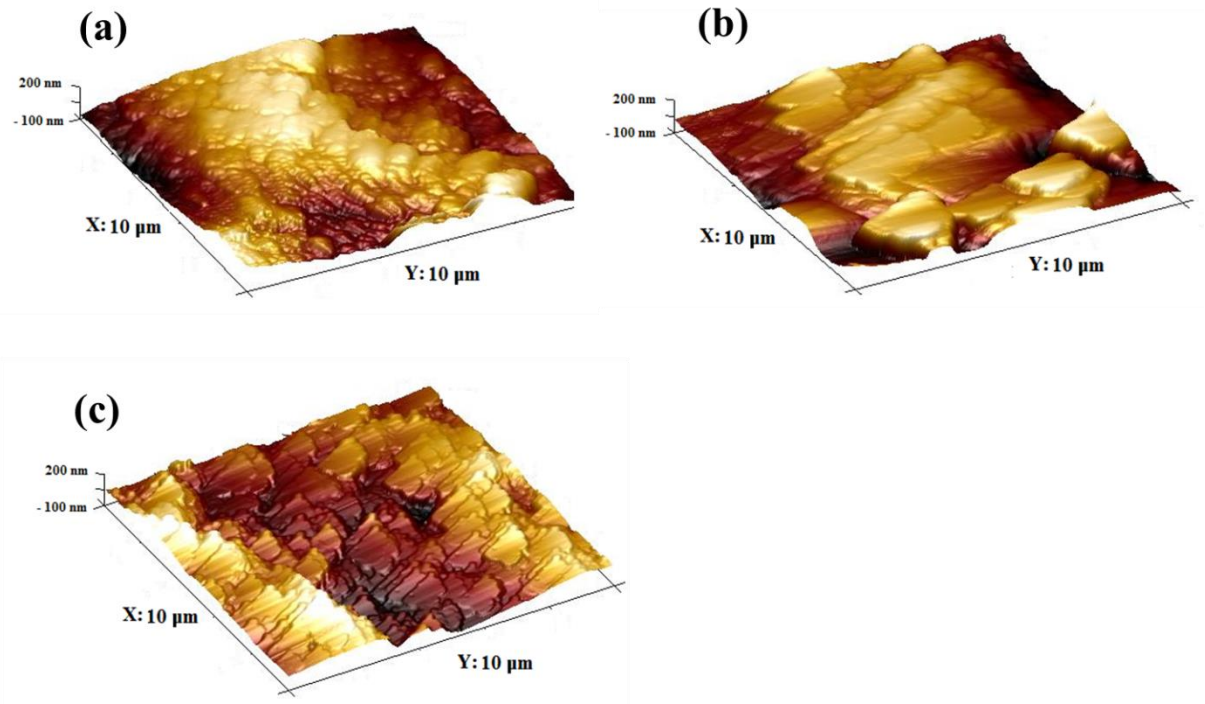
(a)
200 nm
- 100 nm
X: 10 µm
Y: 10 µm
(b)
200 nm
- 100 nm
X: 10 µm
Y: 10 µm
(c)
200 nm
- 100 nm
X: 10 µm
Y: 10 µm

**Figure 4**

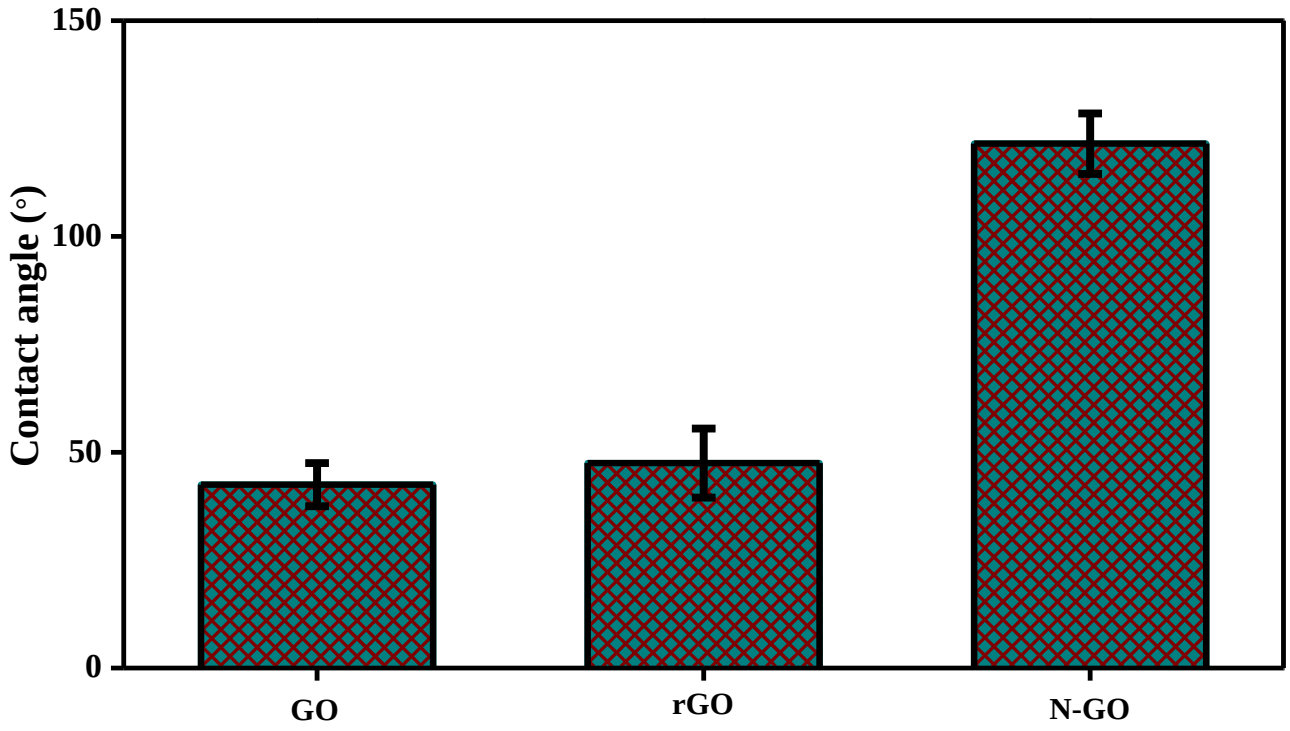

**Figure 5**

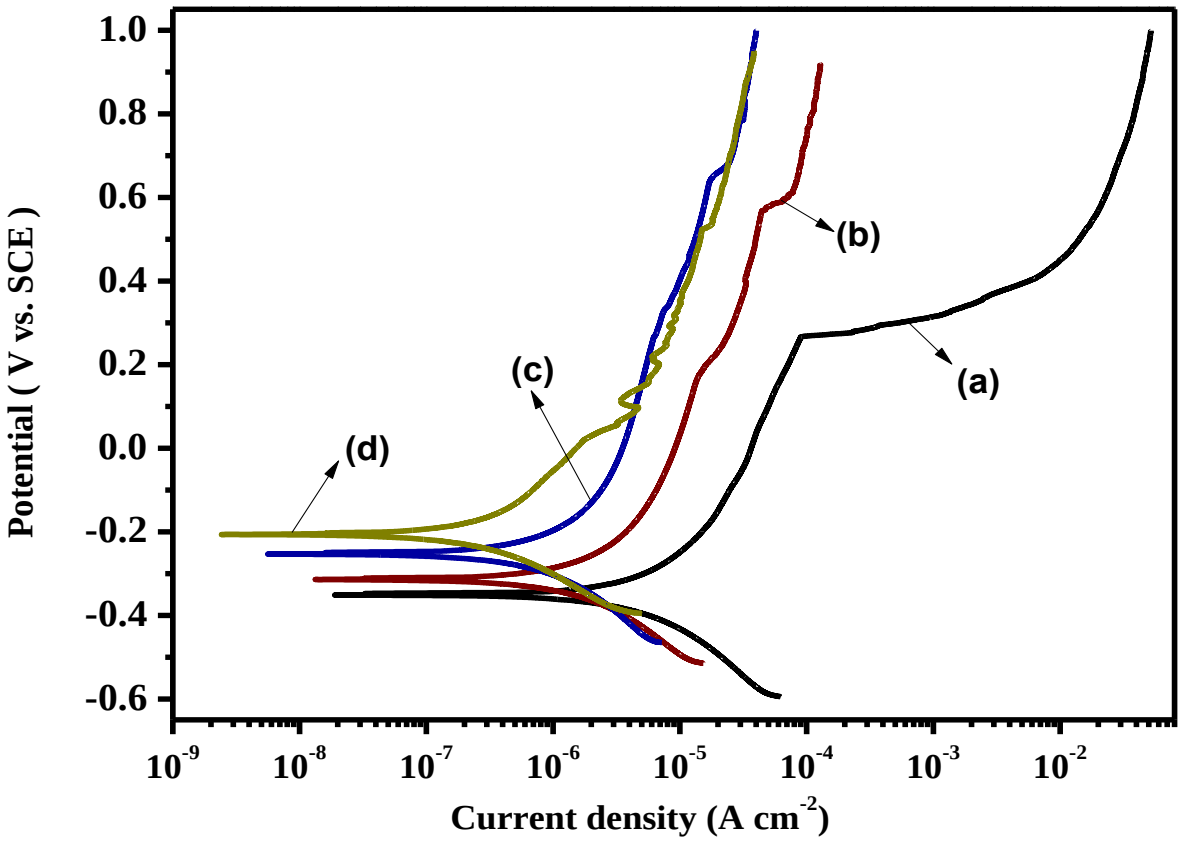
1.0
0.8
0.6
0.4
0.2
0.0
-0.2
-0.4
-0.6
Potential ( V vs. SCE )
10-9
10-8
10-7
10-6
10-5
10-4
10-3
10-2
Current density (A cm-2)
(a)
(b)
(c)
(d)

**Figure 6**

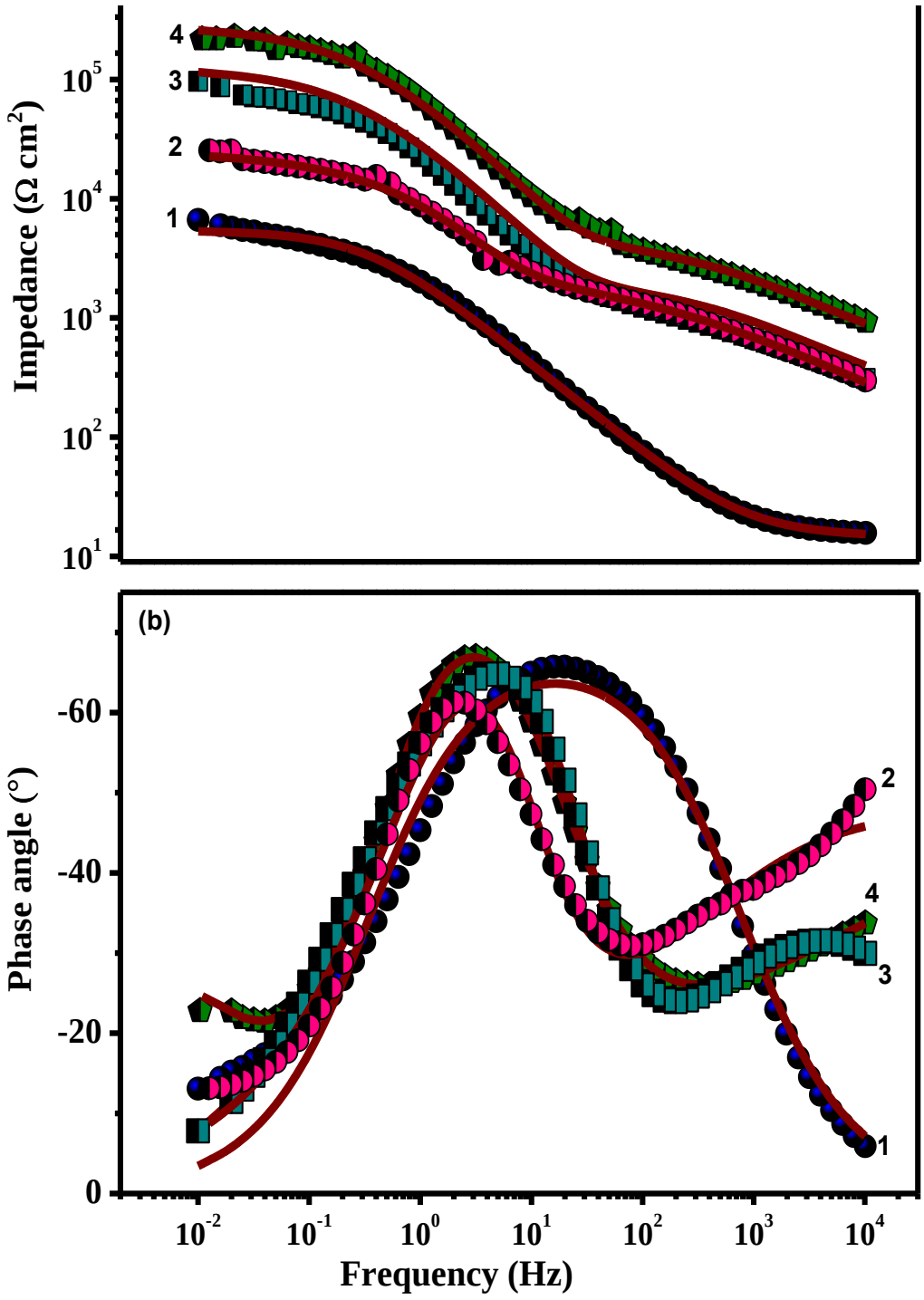
Impedance (Ω cm²)
10⁵
10⁴
10³
10²
10¹
4
3
2
1
(b)
Phase angle (°)
-60
-40
-20
0
10⁻²
10⁻¹
10⁰
10¹
10²
10³
10⁴
Frequency (Hz)
2
4
3
1

**Figure 7**

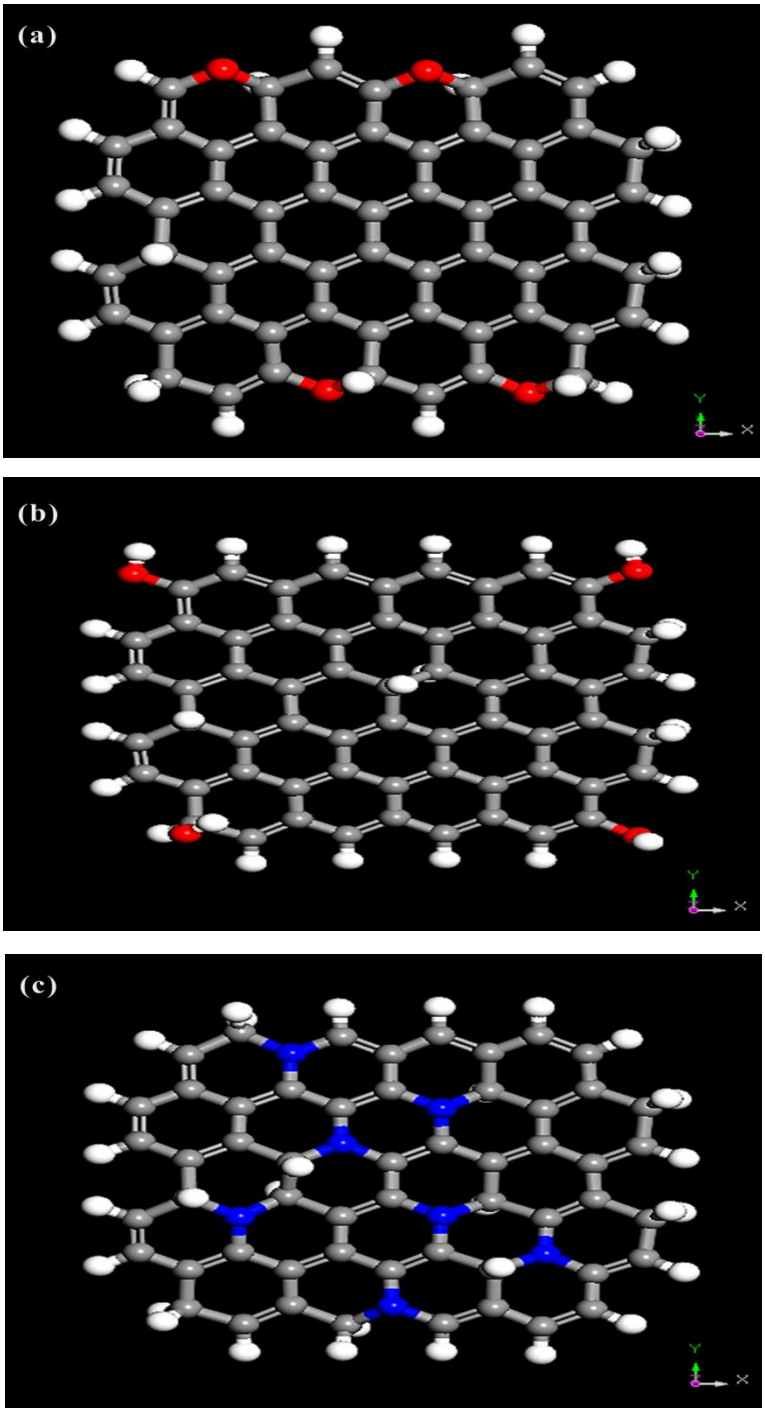

**Figure 8**

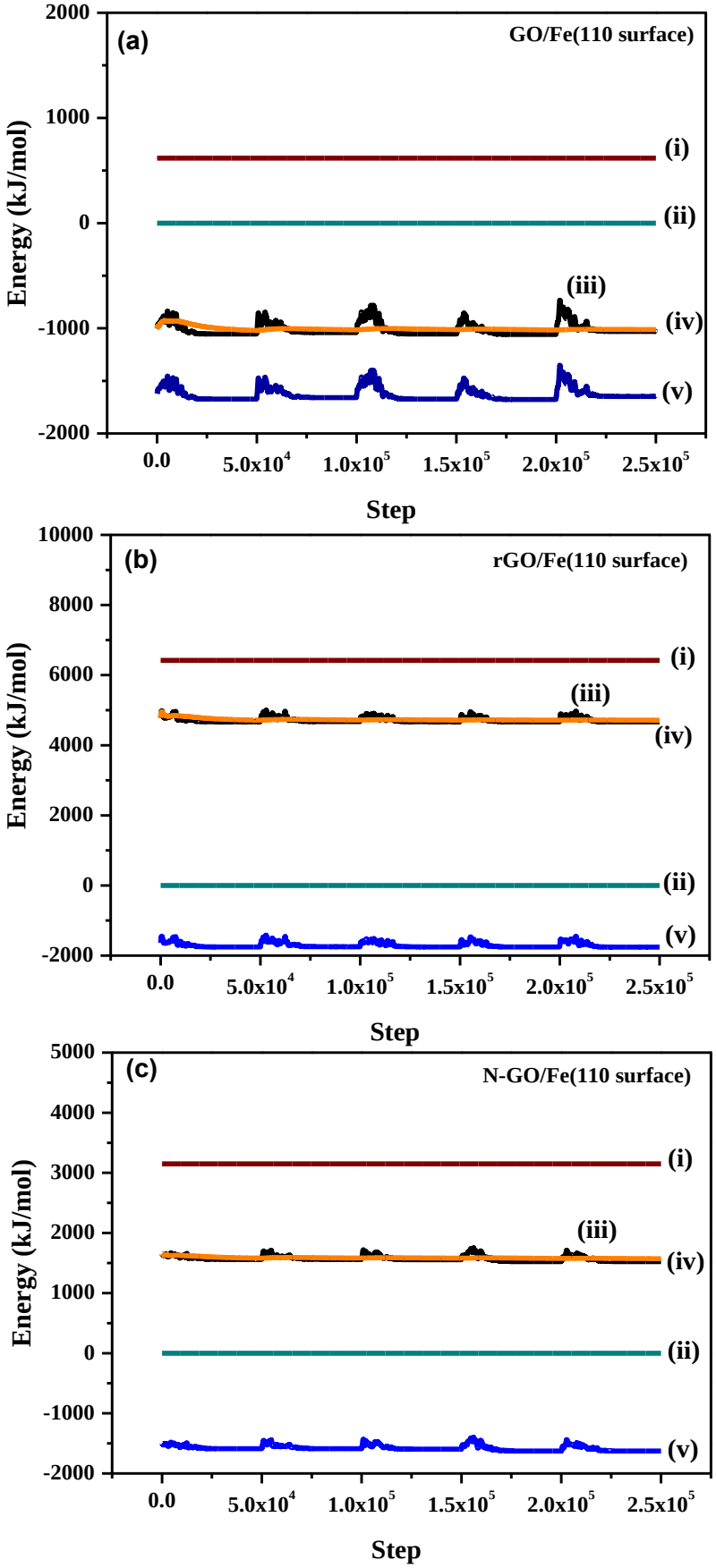
(a)
GO/Fe(110 surface)
Energy (kJ/mol)
2000
1000
0
-1000
-2000
(i)
(ii)
(iii)
(iv)
(v)
0.0
5.0x10^4
1.0x10^5
1.5x10^5
2.0x10^5
2.5x10^5
Step
(b)
rGO/Fe(110 surface)
Energy (kJ/mol)
10000
8000
6000
4000
2000
0
-2000
(i)
(iii)
(iv)
(ii)
(v)
0.0
5.0x10^4
1.0x10^5
1.5x10^5
2.0x10^5
2.5x10^5
Step
(c)
N-GO/Fe(110 surface)
Energy (kJ/mol)
5000
4000
3000
2000
1000
0
-1000
-2000
(i)
(iii)
(iv)
(ii)
(v)
0.0
5.0x10^4
1.0x10^5
1.5x10^5
2.0x10^5
2.5x10^5
Step

**Figure 9**

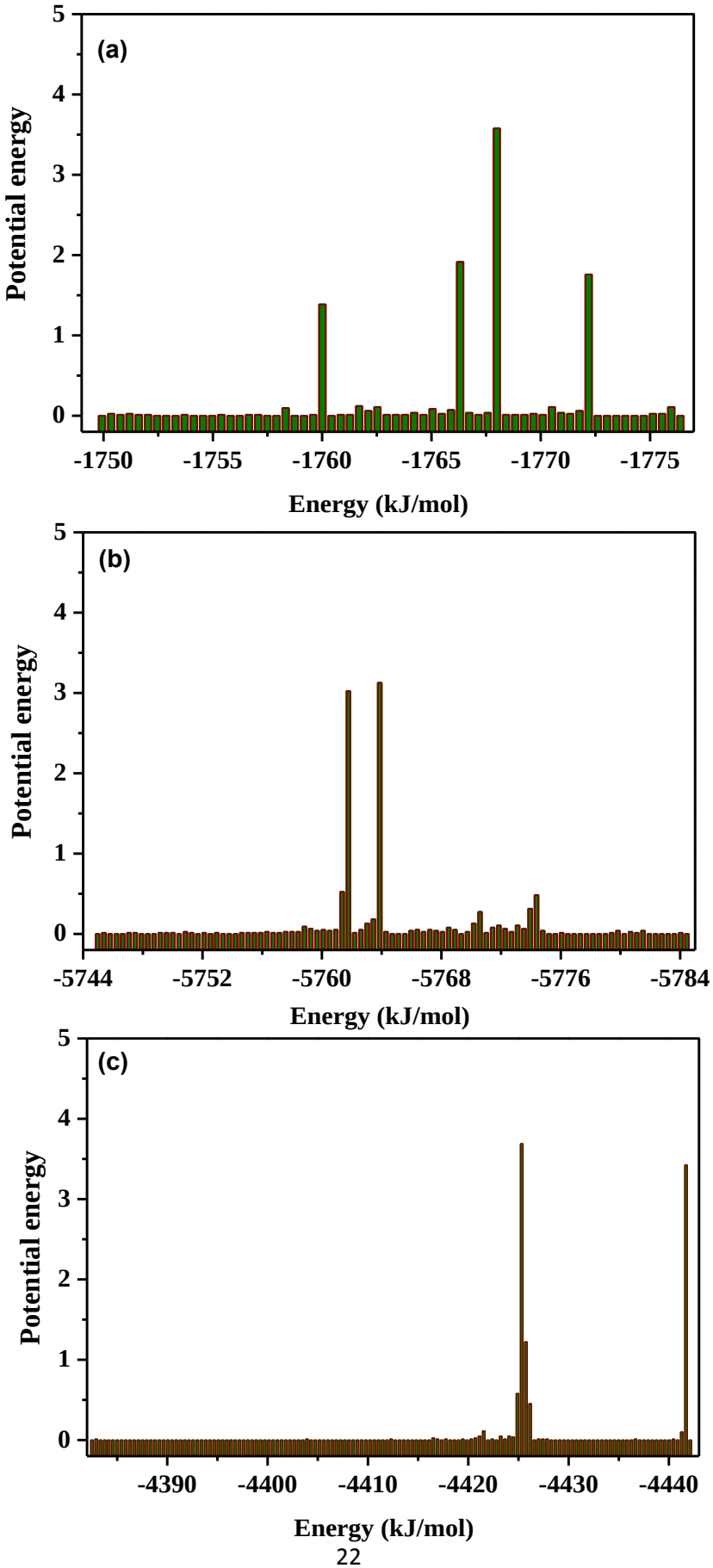
(a)
Potential energy
Energy (kJ/mol)
(b)
Potential energy
Energy (kJ/mol)
(c)
Potential energy
Energy (kJ/mol)

**Figure 10**

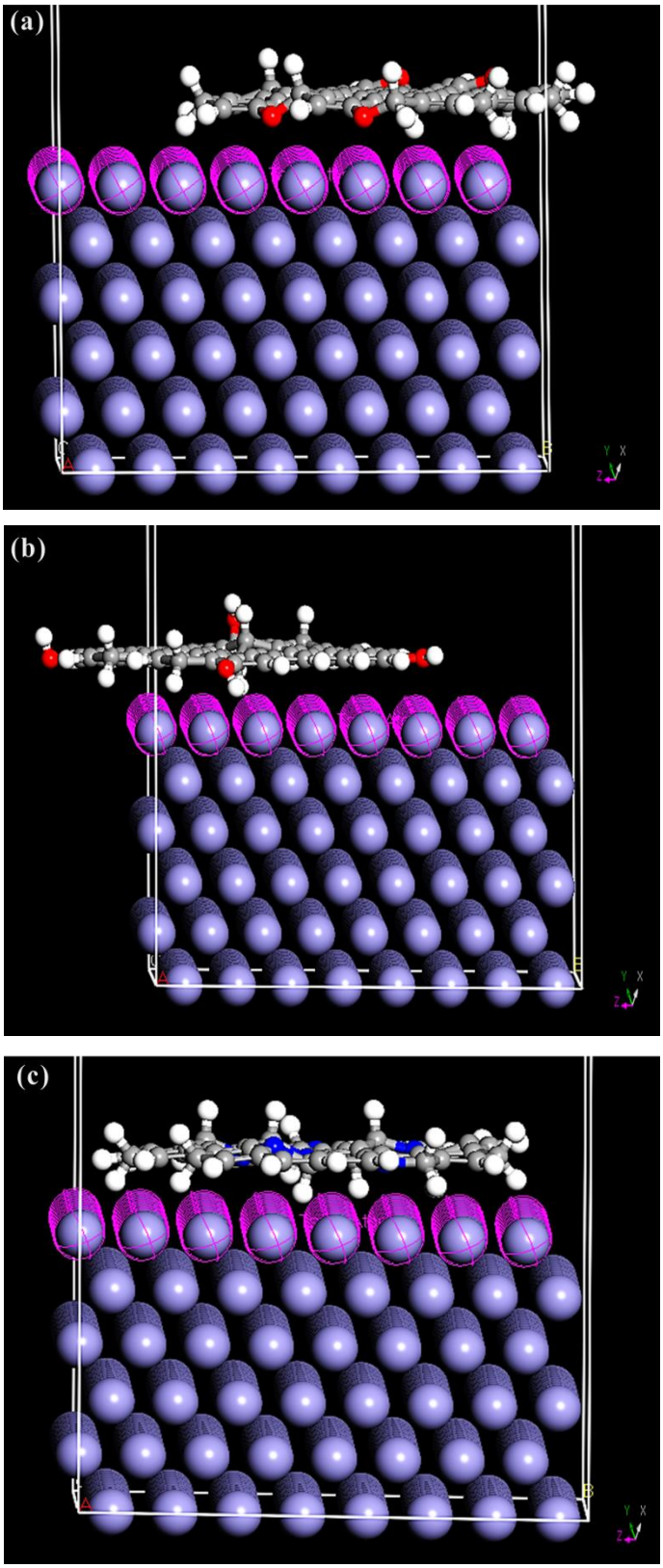

**Table 1**

| S. No. | Substrate | $E_{corr}$ mV | $j_{corr}$ μA cm$^{-2}$ | $\beta_a$ mV/dec | $\beta_b$ mV/dec | $\eta$ (%) | $v$ (mpy) × $10^{-4}$ |
|---|---|---|---|---|---|---|---|
| **1** | **Bare SS** | –0.346 | 5.660 | 58 | 63 | -------- | 1.304 |
| **2** | **GO** | –0.312 | 0.951 | 52 | 39 | 94.34 | 0.0082 |
| **3** | **rGO** | –0.248 | 0.137 | 63 | 53 | 97.52 | 0.0029 |
| **4** | **N-GO** | –0.205 | 0.007 | 56 | 74 | 98.85 | 0.0001 |

**Table 2**

| S. No. | Substrate | $R_s$ Ω cm$^2$ | $R_{ct}$ kΩ cm$^2$ | $Q_{dl}$ μF cm$^{-2}$ | $n_{dl}$ | $R_f$ kΩ cm$^2$ | $Q_f$ μF cm$^{-2}$ | $n_f$ |
|---|---|---|---|---|---|---|---|---|
| **1** | **Bare SS** | 15.37 | 5.93 | 101.1 | 0.85 | ----- | ---- | ----- |
| **2** | **GO** | 23.48 | 21.38 | 24.36 | 0.90 | 5.9 | 13.28 | 0.91 |
| **3** | **rGO** | 48.29 | 96.66 | 19.24 | 0.98 | 6.85 | 9.94 | 0.97 |
| **4** | **N-GO** | 36.24 | 218.34 | 0.93 | 0.98 | 38.63 | 3.35 | 0.97 |

**Table 3**

| Coating | Total Energy | Adsorption energy | Rigid adsorption energy | Deformation energy | $dE_{ad}/dN_i$ |
|---|---|---|---|---|---|
| **GO** | –1132.40 | –1780.89 | –1774.45 | 23.56 | –1780.89 |
| **rGO** | 676.32 | –5745.18 | –1822.38 | –3922.75 | –5745.18 |
| **N-GO** | –1232.82 | –4382.99 | –1754.84 | –2628.15 | –4382.99 |